BIOCHEMISTRY
including biophysical chemistry & molecular biology
Article

Biochemistry **2010,** *49,* 1963–1969 1963
DOI: 10.1021/bi9015605

Structural Basis for Inverting the Enantioselectivity of Arylmalonate Decarboxylase Revealed by the Structural Analysis of the Gly74Cys/Cys188Ser Mutant in the Liganded Form[†,‡]

Rika Obata[§] and Masayoshi Nakasako*[,§,∥]

[§]*Department of Physics, Faculty of Science and Technology, Keio University, 3-14-1 Hiyoshi, Kohoku-ku, Yokohama, Kanagawa 223-8522, Japan, and* [∥]*The RIKEN Harima Institute/SPring-8, 1-1-1 Kouto, Sayo-cho, Sayo-gun, Hyogo 679-5148, Japan*

Received September 7, 2009; Revised Manuscript Received February 2, 2010

ABSTRACT: Arylmalonate decarboxylase catalyzes the enantioselective decarboxylation of α-aryl-α-methylmalonate to produce optically pure α-arylpropionate. The enzyme is comprised of two α/β domains and contains an active site situated between the two domains. The site is formed by Tyr48, Gly74-Thr75-Ser76, Tyr126, and Cys188-Gly189-Gly190 residues. Since it has been observed that the Gly74Cys/Cys188Ser mutation inverts the enantioselectivity of the enzyme, we determined the crystal structure of the Gly74Cys/Cys188Ser mutant in the liganded form at a resolution of 1.45 Å to understand the structural basis for this inversion. The overall structure of the enzyme overlapped well with that of the benzylphosphonate-associated wild-type enzyme, and the mutations had little effect on the structure of the active site. A ligand molecule bound to the active site in an unusual semiplanar conformation resembling the planar enediolate reaction intermediate could be assigned as phenyl acetate. The inversion in enantioselectivity by the paired mutation is explained by the mirror symmetry between Cys74 in the mutant and Cys188 of the wild type with respect to the carbon atom in the ligand to be protonated. Comparison of the wild-type and Gly74Cys mutant crystal structures suggested that ligand binding induces a positional shift of the Cys188-Gly189-Gly190 region toward the Gly74-Thr75 pair which provides two oxyanion holes necessary to stabilize the negatively charged enediolate reaction intermediate. The ligand binding also simultaneously induces the formation of a hydrophobic cluster over the active site cleft. Thus, AMDase is proposed to have "open" and "closed" conformations of the active site that are regulated by ligand binding. These results may provide an effective strategy for the rational design to invert the enantioselectivity of enzymes.

Enantiomerically pure chemicals are important building blocks in organic chemistry and are in increasing demand in chemical and pharmaceutical industries. Enantioselective organocatalysts and asymmetric metal complexes with asymmetric architectures have been developed for the synthesis of chiral products from prochiral substrates with high yields (*1*). Natural evolution has provided a number of enzymes with high enantioselectivities and positional (regio) selectivities suitable for the synthesis of enantiomerically pure compounds with few byproducts (*2*). Enzymes have been used in industrial chemical synthesis under mild conditions, and their use provides benefits for green chemistry.

The weakness of using enzymes stems from the lack of mirror-image enzymes for the formation of either product enantiomer in asymmetric synthesis (*3*). To overcome this, two type of approaches, the direct evolution method (*4*, *5*) and rational design (*6*), have been applied to invert enantiopreference by mutating essential residues in wild-type enzymes. Multiple mutations to change substrate orientation have reversed the enantioselectivity of several enzymes (*6*). One strategy is pairwise mutagenesis to exchange simply catalytic residues in mirror symmetry to the wild type (*6*). Pairwise mutagenesis of industrially interest enzymes has begun, and the applications are reported for oxidase (*7*), elastase (*8*), and decarboxylase (*9*).

Arylmalonate decarboxylase (AMDase,[1] EC 4.1.1.76) from *Alcaligenes bronchisepticus* (*10*) is one of the enzymes to have inverted enantioselectivity through the exchange of key catalytic residues (*9*). Wild-type AMDase catalyzes the enantioselective decarboxylation of prochiral α-aryl-α-methylmalonates to optically pure α-arylpropionates at high enantiometric excess and yields (*11*) and has been shown to be dependent upon the Cys188 residue (*12*). The reaction proceeds through the enantioselective decarboxylation of the substrate and the enantio-face selective protonation of the enediolate intermediate (*10*) (Figure 1A).

[†]This work was supported by grants from MEXT (15076210 and 20050030) and JSPS (1920402) to M.N. The biochemical assays using PA were conducted under the approval of the Kanagawa Prefectural Government.

[‡]The atomic coordinates and the structure factors of the Gly74Cys/Cys188Ser mutant were deposited in the Protein Data Bank as entry 3IXL.

*To whom correspondence should be addressed: Department of Physics, Faculty of Science and Technology, Keio University, 3-14-1 Hiyoshi, Kohoku-ku, Yokohama, Kanagawa 223-8522, Japan. Telephone: (81)-45-566-1713. Fax: (81)-45-566-1672. E-mail: nakasako@phys.keio.ac.jp.

[1]Abbreviations: AMDase, arylmalonate decarboxylase; β-ME, β-mercaptoethanol; BnzPO, benzylphosphonate; BrPA, α-bromophenylacetate; H-bond, hydrogen bond; HPLC, high-performance liquid chromatography; MR, molecular replacement; PA, phenylacetate; PDB, Protein Data Bank; PEG5000, polyethylene glycol 5000; PM, phenylmalonate; rmsd, root-mean-square deviation.

Published on Web 02/05/2010

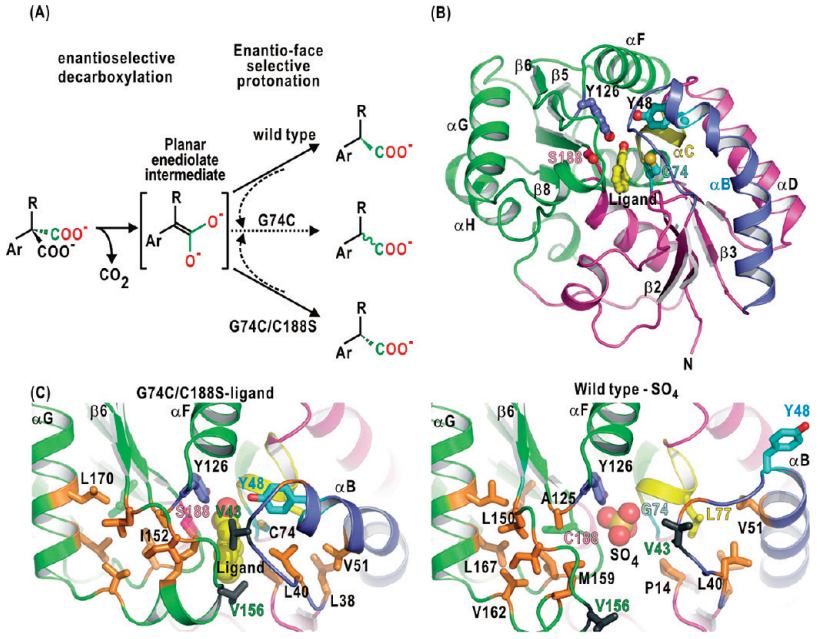

FIGURE 1: (A) Enzymatic reactions catalyzed by wild-type AMDase (*10*), the Gly74Cys/Cys188Ser double mutant (*9*), and the Gly74Cys mutant (*16*). Prochiral substrates are enantioselectively decarboxylated by the wild-type and double mutant AMDases. The products of the double mutant have an opposite chirality versus that of the wild-type enzyme. The dotted lines indicate the racemization of chiral α-substituted α-arylacetates by the Gly74Cys mutant. The planar enediolate intermediate expected for both the decarboxylation and racemization reactions is shown in brackets. (B) Crystal structure of the Gly74Cys/Cys188Ser mutant in the liganded form. The N-terminal (residues 1−103 and 211−230) and C-terminal domains (residues 104−210 and 231−240) are colored pink and green, respectively. Helix αB (residues 45−65) (blue) displays a large bend in the liganded state. Helix αC (yellow) contributes to the binding of the ligand through the residues of the N-terminal face. The colored stick models represent the side chains of the key residues for ligand binding (Tyr48, Gly74, Cys74, Cys188, Ser188, and Tyr126). (C) Hydrophobic cluster surrounding the active sites of the liganded Gly74Cys/Cys188Ser mutant (left) and SO_4-associated wild-type enzyme (right). The panels illustrating the molecular structures were generated using PyMol (*37*).

AMDase consists of compact N- and C-terminal domains with an α/β fold (*13*). The crystal structures of PO_4- and benzylphosphonate (BnzPO)-associated wild-type enzymes demonstrate that the active site is formed by the Cys188−Gly190 loop, Gly74-Thr75-Ser76, and Tyr126 (*14*, *15*). The Gly74Cys/Cys188Ser mutant enzyme produces an arylpropionate of the opposite enantiomorph versus that produced by the wild type (*9*). In addition, a Gly74Cys mutation results in an enzyme catalyzing the racemization of α-arylpropionate (*15*).

Here, we determined the crystal structure of a Gly74Cys/Cys188Ser AMDase mutant in the liganded form at a resolution of 1.45 Å to reveal the structural requirements for inversion in the enantioselective reaction. The Cys74 side chain in the mutant is in the mirror symmetry versus the Cys188 side chain in the wild-type enzyme. Through a comparison to known AMDase structures, we propose that ligand binding induces an open−close motion of the active site cleft that is responsible for the enantio-face selective protonation.

MATERIALS AND METHODS

Protein Purification and Crystallization. The Gly74Cys/Cys188Ser mutant and the wild-type AMDase were overexpressed in *Escherichia coli* and purified to homogeneity according to the reported procedures (*16*, *17*). The purified enzymes were concentrated to 20 mg/mL in a buffer containing 10 mM Tris-HCl, 0.5 mM EDTA, and 5 mM β-mercaptotheanol (β-ME) (pH 8.0). Crystallization of the Gly74Cys/Cys188Ser mutant enzyme was performed by the hanging-drop vapor-diffusion method at 293 K. Crystals appeared as stacked plates when a precipitant solution containing 1.2 M ammonium sulfate, 15% (w/v) polyethylene glycol 5000 (PEG5000), 10 mM bromophenylacetate (BrPA), 1% (v/v) dioxane, and 70 mM HEPES (pH 7.6) was used.

X-ray Diffraction Data Collection, Structure Determination, and Refinement. X-ray diffraction data of Gly74Cys/Cys188Ser mutant crystals were collected at BL26B1 (*18*) of SPring-8 via the mail-in system (*19*). The X-ray wavelength was 1.0000 Å, and a MAR CCD225 detector was used. Crystals harvested from hanging drops were set in micro dialysis cells filled with precipitant solution. Then, they were dialyzed against a cryo buffer containing 2.2 M ammonium sulfate, 22% (w/v) glycerol, 5 mM BrPA, and 0.25% (w/v) ethanol (pH 6.5) for 12 h. The collected diffraction data were processed using the HKL2000 suite (*20*) (Table 1). In the crystal, one mutant molecule occupied the crystallographic asymmetric unit.

The crystal structure of the mutant was determined by the molecular replacement (MR) method with AMoRe (*21*) in the CCP4 suite (*22*). We used the crystal structure of the wild-type enzyme (Supporting Information, PDB entry 3DTV) as the search model. Crystallographic structure refinement was performed for the MR solution using Refmac5 (*23*). The model was constructed using turboFRODO (BioGraphics) and difference Fourier electron density maps calculated in every refinement round. The statistics of the refined model are listed in Table 1. The main chain dihedral angle of Ser188 was in a disallowed region in the Ramachandran plot because of interactions with a ligand molecule bound to the active site (see the Results). Stereochemical restraints for the ligand were prepared using the libcheck program in the CCP4 suite.

Measurements of Enzymatic Kinetics. The decarboxylation of phenylmalonate (PM) by wild-type AMDase was measured in the presence of phenylacetate (PA). Prior to the reaction,

Table 1: Data Collection and Refinement Statistics for the Gly74Cys/Cys188Ser Mutant

Data Collection	
space group	$P2_12_12$
unit cell parameters a, b, c (Å)	38.39, 63.35, 82.41
resolution (Å)	100−1.45 (1.48−1.45)[a]
no. of observed/unique reflections	370811/35026
completeness (%)	95.8 (70.8)[a]
$\langle I/\sigma_I \rangle$	28.83 (5.14)[a]
R_{merge}[b]	0.054 (0.246)[a]
Refinement	
resolution (Å)	20.00−1.45
no. of reflections	33171
R_{work}[c]	0.172
R_{free}[d]	0.194
no. of atoms	
protein	1703
ligand and ion	21
water	248
average B factor (Å^2)	
protein	10.8
ligand and ion	30.7
water	28.9
rmsd from ideal geometry[e]	
bond lengths (Å)	0.007
bond angles (deg)	1.319
Ramachandran regions (%)[f]	
most favored	93.8
additionally allowed	5.2
generously allowed	0.5
disallowed	0.5 (Ser188)[g]

[a]Values in parentheses are for the highest-resolution shell. [b]$R_{merge} = \sum_{hkl}\sum_i |I_i(hkl) - \langle I(hkl)\rangle| / \sum_{hkl}\sum_i I_i(hkl)$, where $I_i(h)$ is the intensity of the ith observation of reflection hkl. [c]$R_{work} = \sum_h |F_{obs}(h) - F_{calc}(h)| / \sum_h F_{obs}(h)$, where $F_{obs}(h)$ and $F_{calc}(h)$ are the observed and calculated structure factors, respectively, of reflection h. [d]The R_{free} factor was calculated for the 5% of unique reflections that were not used in the structure refinement throughout (*35*). [e]Root-mean-square deviations from the ideal stereochemical geometry. [f]Distribution of Ramachandran angles according to PROCHECK (*36*). [g]The dihedral angle of the Ser188 main chain is distorted by the contacts between the side chain and the ligand.

a 480 μL solution of 0.15 μM AMDase in 10 mM Tris-HCl (pH 8.5) was mixed with 60 μL of a 23, 45, 90, or 180 mM PA solution and the mixture was incubated for 30 min. The decarboxylation reaction was initiated by addition of 60 μL of a 100 mM PM solution. After 10 min, the reaction was quenched by addition of 10 μL of 1 M HCl. The amount of PM and PA remaining in the quenched solution was quantitatively analyzed by a Gold high-performance liquid chromatography (HPLC) system (Beckman) with an ULTRASPHERE ODS column (Beckman). The system was operated at a flow rate of 1 mL/min, and the eluate was monitored by absorption at 254 nm. The eluant contained 10% (v/v) aqueous acetonitrile and 0.05% (v/v) trifluoroacetate. Under the operating conditions, the retention time of the PM substrate was 3.2 min, while PA appeared 4.8 min after injection. The relationship between reaction velocity and the amount of synthesized PA was calculated by subtracting the initial amount (before the reaction) from the amount remaining in the quenched solution.

The absorption spectra of all enzymes, PA, PM, and their mixtures were recorded at 298 K in quartz cells using a Hitachi U-2001 UV−vis spectrophotometer.

RESULTS

Structure of the AMDase Gly74Cys/Cys188Ser Mutant. The crystal structure of the Gly74Cys/Cys188Ser mutant with a ligand molecule bound to the active site was refined at a resolution of 1.45 Å (Figure 1B). The structure of the double mutant was very similar to those of the PO_4-associated (*14*) and BnzPO-associated wild-type enzymes (*15*) as indicated by the root-mean-square deviation (rmsd) of CA atoms of ca. 0.25 Å, despite the different molecular packing modes of their crystals. However, the double mutant displayed conformational differences in both the active site and helix αB when compared to the wild-type and Gly74Cys mutant enzymes in the SO_4-associated state (Supporting Information). Helix αB of the double mutant bends at Ser54 and extends to the Glu46−Tyr48 region, which is in a loop conformation in SO_4-associated enzymes (Figure 1C). Accompanying the bend, the Tyr48 side chain travels ca. 18 Å from its position in the SO_4-associated form.

Above the active site cleft, Val43 of the β2−αB loop contacts Thr154 and Val156 of the β6−αG loop which induces the formation of a hydrophobic cluster covering the active site. However, in the SO_4-associated wild-type and Gly74Cys mutant enzymes, these two loops are separated from each other and the hydrophobic cluster is not observed (Figure 1C). Considering the structural similarity between the liganded double mutant and the BnzPO-associated wild-type enzyme, the conformational differences observed are likely induced by ligand binding rather than artifacts of crystallization. Thus, AMDase possibly adopts the "open" conformation in the unliganded or SO_4-associated forms and the "closed" conformation when bound to ligand.

Structure of the Mutant Active Site. The active site structure of the Gly74Cys/Cys188Ser mutant was unambiguously modeled from the clear electron density map (Figure 2A,B). From this model, we observed that the Cys74 residue was free from the β-ME modification found for Cys188 of the wild-type enzyme crystallized in the presence of β-ME (*13*). In addition, the side chains of Pro14, Tyr48, Cys74, and Leu77 formed a hydrophobic pocket together with the N-terminal face of helix αC, and the active site of the double mutant could be superimposed on those of the PO_4- and BnzPO-associated wild-type enzymes (*14*, *15*) (Figure 2C). The Ser188 side chain was in the same conformation as that of Cys188, and Cys74 was just fit to that in the Gly74Cys mutant (Figure 2D). In the closed conformation of the active site, the side chains of Cys188 and Ser188 face the crevice, while in the open conformation, the Cys188 side chains are confined to the hydrophobic pocket (Figure 2D,E). Ligand binding is thought to induce the rotation of the main chain of Cys188 (or Ser188) and its movement toward the Gly74 (or Cys74) residue.

The crystal structure analysis of the double mutant revealed an unknown ligand molecule was bound to the active site. The electron density of the molecule suggested that it was composed of a phenyl group (atoms C1−C6), a carboxyl group (atoms O1, C, and O2), and a carbon atom (Cα) that connected the two groups (Figure 2A). We also determined that the molecule had a semiplanar conformation with a slight twist at the Cα atom with a C2−C1−Cα−C dihedral angle of 29.0° and resembled the enediolate form of PA (Figure 2B). The structure model suggests a distorted sp^2 hybridization rather than sp^3, and it should be noted that the electron density was never approximated as the mixture of electron density from PA in the sp^3 hybridization and the enediolate intermediate in the sp^2 hybridization.

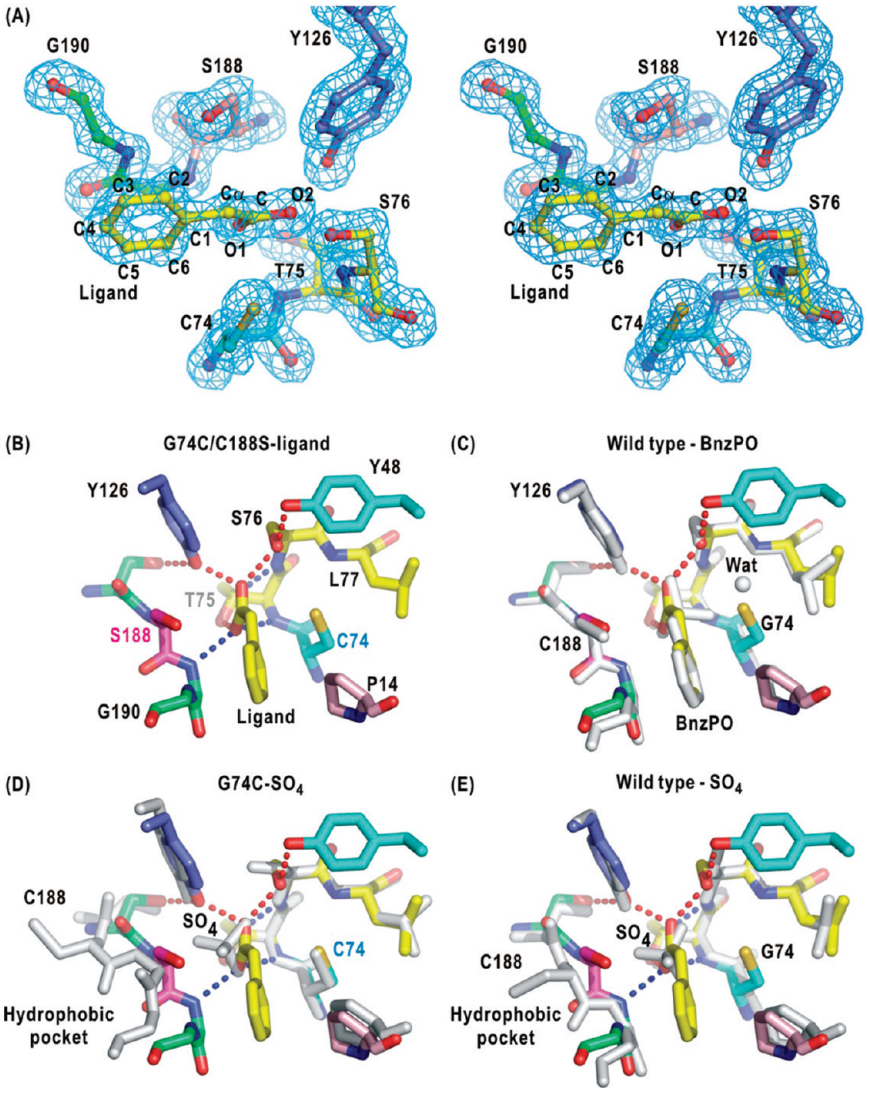

FIGURE 2: (A) Stereoplot illustrating the structure of the active site in the liganded Gly74Cys/Cys188Ser mutant. The blue fish net represents the omit-refined $F_{obs} - F_{calc}$ difference Fourier electron density map calculated using the reflections between the Bragg spacing of 20.0 and 1.45 Å and contoured at the 4.0σ level from the average. The ligand atoms are labeled as a reference for Table 2. (B) Stick model representing the active site of the double mutant as depicted in panel A. The dotted red lines represent H-bonds formed around the carboxylate group of the ligand, while dotted blue lines denote the contributions of the NH groups of the oxyanion holes toward neutralizing the carboxylate groups. The liganded active site structure is compared with the active site structures of the BnzPO-associated wild-type enzyme (PDB entry 3IP8) (*15*) (C), the SO_4-associated Gly74Cys mutant (D), and the SO_4-associated wild-type enzyme (PDB entry 3DTV). The structures are superimposed so that the residues forming the N-terminal face of helix αC optimally overlap.

The semiplanar conformation of the ligand is unusual considering that $C_2-C_1-C\alpha-C$ dihedral angles of 60−90° are usually observed in PA molecules bound to other enzymes (*24*−*27*).

The unusual ligand conformation was stabilized by six hydrogen bonds (H-bonds) and 12 van der Waals contacts (Figure 2B and Table 2). The four interacting pairs (O1−Thr75 NH, O1−Gly189 NH, O2−Tyr126 OH, and O2−Ser76 OG) are far from the ideal H-bond angle (*28*), suggesting that the Thr75 NH and Gly189 NH pair in particular provides an oxyanion hole to stabilize the enediolate intermediate as well as the Tyr126 OH and Ser76 O pair, as supported by a previous report (*14*). The phenyl ring of the ligand was shown to contact Pro14, Gly189, and Gly190 (Figure 2B and Table 2).

Enzymatic Activity of AMDase in the Presence of Phenylacetate. The strong interactions between the active site residues and the ligand caused an unfavorable main chain dihedral angle in Ser188, and the thermal factors of the ligand atoms were comparable with those of the active site residues. Taken together, these findings suggested that the ligand molecule acted as an inhibitor of AMDase. The ligand had the chemical composition of PA and resembled the structure of the planar enediolate intermediate expected in the decarboxylation of PM (Figures 1A and 3A), although PM was absent from the crystallization buffer. However, BrPA degrades to several components that likely include PA during the crystallization process as determined by HPLC (data not shown). While PA was not a substrate for either the wild type or the double mutant, its inhibitory activity for the enzymes was unknown.

In the presence of increasing concentrations of PA added prior to the reaction, the apparent reaction velocity in the decarboxylation of PM by wild-type AMDase was shown to decrease (Figure 3B). The amount of PA produced from PM was very small when the concentration of PA reached 20 mM against 0.15 mM AMDase. This indicates that PA possesses an inhibitory activity on this enzyme.

Table 2: Interactions in the Active Site Cleft of the Liganded Gly74Cys/Cys188Ser Mutant

Ligand−Protein Interactions[a]				
ligand atom	protein atom	distance (Å)	angle (deg)	
O1	Thr75 N	2.99	Thr75 N···O1−C	101.9
	Thr75 OG1	2.81	Thr75 OG1···O1−C	124.5
	Gly189 N	2.80	Gly189 N···O1−C	124.4
O2	Ser76 N	2.84	Ser76 N···O2−C	122.8
	Ser76 OG	2.67	Ser76 OG···O2−C	127.8
	Tyr126 OH	2.67	Tyr126 OH···O2−C	120.1
Cα	Cys74 SG	3.50		
	Ser188 OG	3.70		
C3	Gly190 CA	3.49		
C4	Gly190 CA	3.52		
	Gly190 N	3.60		
C5	Pro14 CD	3.58		
	Pro14 CG	3.45		
	Gly190 N	3.59		
	Gly189 C	3.42		
C6	Pro14 CG	3.62		
	Gly189 C	3.68		
C	Tyr126 OH	3.48		
Among Protein Atoms[a]				
protein atom	protein atom	distance (Å)	angle (deg)	
Tyr48 OH	Ser76 OG	2.62	Tyr48 CZ−Tyr48 OH···Ser76 OG	99.6
Tyr126 OH	Thr75 CB	3.58		
Ser187 OG	Thr75 OG1	2.81	Ser187 CB−Ser187 OG···Thr75 OG1	139.4

[a]The upper limits to pick up H-bonds and van der Waals contacts are 3.4 and 3.7 Å, respectively.

The absorption spectrum of the mixture containing the wild-type enzyme and PM displayed an absorption maximum of ca. 330 nm (Figure 3C). The absorption maximum of a π-electron system shifts to longer wavelengths when the π-electron system expands to a larger area. Thus, the observed spectra suggest that the bound substrate PM or the re-bound PA has a π-electron system larger than that in the phenyl rings of PM or PA in solution. The mixture of the double mutant and PA displayed an absorption maximum very similar to that of the mixture of the wild type and PM (Figure 3D), suggesting the binding of PA to the active site of the double mutant as deduced from the crystal structure described above. If we assume the molar extinctions of liganded PA are comparable between the experiments shown in panels C and D of Figure 3, the absorption data imply that the wild-type AMDase tends to form the PA-liganded state more frequently (~60 times) than the double mutant in the steady state, taking the absorption at 330 nm and the concentrations of the enzymes and ligands used.

No crystals appeared when crystallization buffer was used for the wild-type AMDase enzyme. The results from the steady state kinetics and crystallization suggested that the mutated active site may be advantageous for capturing and holding PA versus the wild-type active site and that the wild-type active site is suitable for catching and releasing PA more frequently than the mutated active site. In addition, when BrPA in the crystallization buffer was replaced with PA, the double mutant failed to crystallize. It is difficult to deny the possibility that the chemical components from the degradation of BrPA induce or help the nucleation of the liganded double mutant.

DISCUSSION

The crystal structure of the Gly74Cys/Cys188Ser mutant was determined in a liganded form at a resolution of 1.45 Å (Figures 1

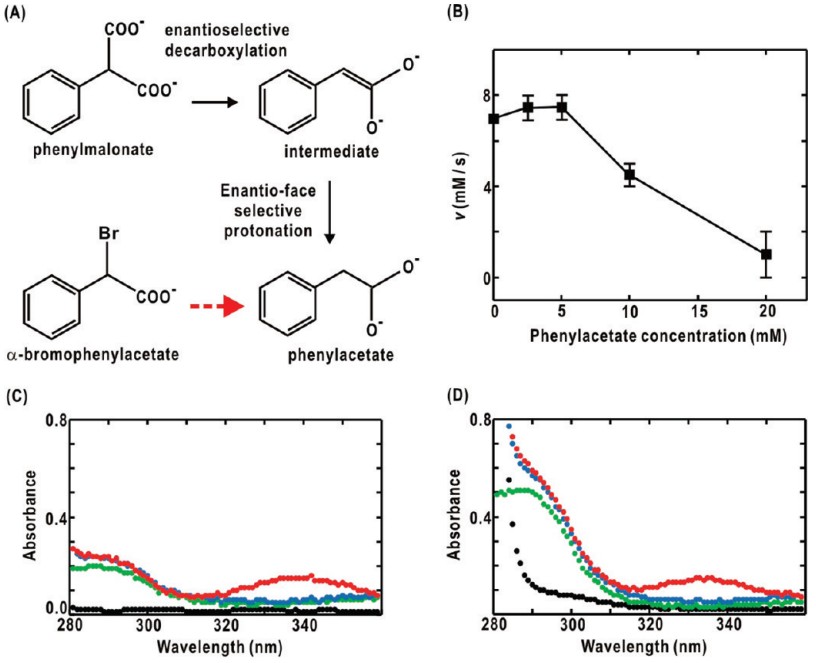

FIGURE 3: (A) Reaction scheme for the decarboxylation of PM. (B) Reaction velocities in the decarboxylation of PM by wild-type AMDase in the presence of PA. The error bars were calculated from the data of three independent experiments. (C) Absorption spectra of the mixture of the wild-type enzyme (1.5 μM) and PM (0.1 mM) in 10 mM Tris-HCl (pH 8.6). The blue dots show the spectrum measured when the enzyme and the compound solutions were mixed, and red dots show the spectrum measured 10 min after the mixing. The green and black dots show the spectra of the enzyme and the compound in Tris buffer at the same concentrations with the mixture. (D) Absorption spectra of the Gly74Cys/Cys188Ser mutant (3.9 μM) and PA (3 mM) in 10 mM Tris-HCl (pH 8.6). The coloring scheme is the same as that in panel C.

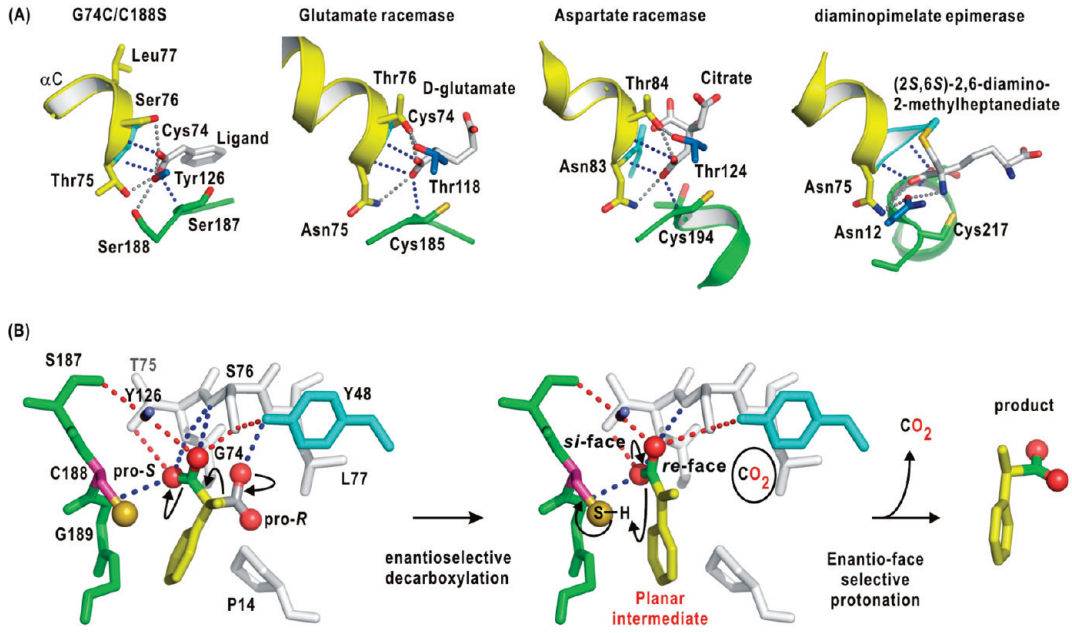

FIGURE 4: (A) Comparison of the active site structures of the liganded Gly74Cys/Cys188Ser mutant AMDase and glutamate racemase (PDB entry 1ZUW) (*29*), Cys82Ala mutant aspartate racemase (PDB entry 2DX7) (*30*), and diaminopimelate epimerase (PDB entry 2GKE) (*31*). The dotted gray lines represent possible H-bonds between the ligand and the active site residues, while the dotted blue lines indicate the contribution from the NH groups forming the N-terminal face of helices corresponding to αC in AMDase. (B) Schematic illustration for the proposed substrate binding mode and enantioselective decarboxylation of 2-methyl-2-phenylmalonate by the wild-type AMDase.

and 2 and Table 1). The ligand was assigned as PA and possessed a semiplanar conformation resembling the enediolate intermediate expected in the decarboxylation of PM (Figures 2 and 3). These results allow us to speculate about how the double mutation enables the inversion of enantioselectivity and propose the ligand binding mode and reaction scheme.

First, it should be noted that the ligand binding mode in the active site of the double mutant is similar to those reported in representative enzymes of the enolase family (Figure 4A) (*29*−*31*). In this family, the carboxylate group of the ligand forms H-bonds with either Asn or Thr residues on the N-terminal face of a helix, which in AMDase corresponds to helix αC. The carboxylate group also binds to an oxyanion hole formed between the N-terminal face of the helix and the loop located at the opposite side of the active site cleft.

Considering the similarities of ligand binding in the enolase family, we propose a binding mode for 2-methyl-2-phenylmalonate, a model substrate of AMDase, which is illustrated in Figure 4B. In this model, the phenyl ring of the substrate is sandwiched among the Gly189-Gly190 pair, Gly74, and Pro14, and the dicarboxylate group contacts Tyr48, Gly74, Thr75, Ser76, Tyr126, and Gly189. The binding mode and the arrangement of the active site residues limit the size of the substrate and explain why AMDase binds only ligands with Cα substituents smaller than ethyl and aryl groups smaller than naphthyl (*10*, *12*).

In the proposed binding mode, the decarboxylation at the pro-*R* side is driven by the stereoelectronic effect (*32*) and/or the hydrophobic destabilization in the hydrophobic pocket formed by the Gly74, Lue77, and Tyr48 side chains (*14*). The CO_2 molecule produced by the decarboxylation possibly remains in the pocket until the Tyr48 side chain moves away. Though an enediolate intermediate is expected in the enantioselective decarboxylation (*10*, *14*), AMDase has no metal ion and/or electron sink in the active site unlike enzymes producing enediolate reaction intermediates (*33*, *34*). Thus, the oxyanion holes formed by Gly74, Thr75, Ser76, Tyr126, and Gly189 contribute to the neutralization of the negative charge of the enediolate intermediate, as previously proposed (*14*).

In this binding mode, the enantio-face selective protonation, i.e., the chirality of the final product, depends simply on the location of the reactive SH group of Cys188 or Cys74 relative to the substrate Cα atom to be protonated. For example, in the wild-type enzyme, Cys188 located on the *si* face protonates the enediolate intermediate to give (*R*)-2-phenylpropionate. The Gly74Cys mutant has two cysteine residues, Cys74 and Cys188, on the *si* and *re* faces of the intermediate whose side chains are expected to be in the free thiol state rather than thiol−thiolate pairs. Therefore, these two residues are thought to act as proton donors to produce racemic products. In the Gly74Cys/Cys188Ser double mutant, the Cys74 side chain is in mirror symmetry versus the Cys188 side chain of the wild-type enzyme with regard to the Cα atom of the enediolate intermediate. Thus, the thiol group of the Cys74 side chain protonates the intermediate from the *re* face, while the hydroxyl group of Ser188 protonates the intermediate from the *si* face.

One approach to designing an enzyme with inverted enantioselectivity is to move essential residues to the opposite face of the active site that binds the substrate (*6*). Our crystal structure of the AMDase double mutant demonstrates that this strategy allows the rational design of enzymes if the active site conformation of an enzyme is unchanged by mutations for the inversion.

ACKNOWLEDGMENT

We are grateful to Prof. M. Yamamoto, Dr. N. Dohmae, and Dr. H. Miyatake of RIKEN for their help in the X-ray diffraction experiments and Dr. G. Newton for his careful reading of and comments about the manuscript. We also thank Prof. H. Ohta and Dr. K. Miyamoto of Keio University for their help in sample preparation.

SUPPORTING INFORMATION AVAILABLE

Crystal structures of the wild-type enzyme without β-ME modification of the Cys188 residue and the Gly74Cys mutant. This material is available free of charge via the Internet at http://pubs.acs.org.

REFERENCES

1. Gaunt, M. J., Johansson, C. C. C., McNally, A., and Vo, N. T. (2007) Enantioselective organocatalysis. *Drug Discovery Today 12*, 8–27.
2. Miguel, D., Toscano, T., Woycechowsky, K. J., and Hilvert, D. (2007) Minimalist active-site redesign: Teaching old enzymes new tricks. *Angew. Chem., Int. Ed. 46*, 3212–3236.
3. Gerlt, J. A., and Babbitt, P. (2009) Enzyme (re)design: Lessons from natural evolution and computation. *Curr. Opin. Chem. Biol. 13*, 1–9.
4. May, O., Nguyen, P. T., and Arnold, F. H. (2000) Inverting enantioselectivity by directed evolution of hydantoinase for improved production of L-methionine. *Nat. Biotechnol. 18*, 317–320.
5. Cherry, J. R., and Fidantsef, A. L. (2003) Directed evolution of industrial enzymes: An update. *Curr. Opin. Biotechnol. 14*, 438–443.
6. Mugford, P. F., Wagner, U. G., Jiang, Y., Faber, K., and Kazlauskas, R. J. (2008) Enantiocomplementary enzymes: Classification, molecular basis for their enantiopreference, and prospects for mirror-image biotransformations. *Angew. Chem., Int. Ed. 47*, 8782–8793.
7. van den Heuvel, R. H. H., Fraaije, M. W., Ferrer, M., Mattevi, A., and van Berkel, W. J. H. (2000) Inversion of stereospecificity of vanillyl-alcohol oxidase. *Proc. Natl. Acad. Sci. U.S.A. 97*, 9455–9460.
8. Bartsch, S., Kourist, R., and Bornscheuer, U. T. (2008) Complete inversion of enantioselectivity towards acetylated tertiary alcohols by a double mutant of *Bacillus subtilis* Esterase. *Angew. Chem., Int. Ed. 47*, 1508–1511.
9. Ijima, Y., Matoishi, K., Terao, Y., Doi, N., Yanagawa, H., and Ohta, H. (2005) Inversion of enantioselectivity of asymmetric biocatalytic decarboxylation by site-directed mutagenesis based on the reaction mechanism. *Chem. Commun. 239*, 877–879.
10. Miyamoto, K., and Ohta, H. (1992) Purification and properties of a novel arylmalonate decarboxylase from *Alcaligenes bronchisepticus* KU1201. *Eur. J. Biochem. 210*, 475–481.
11. Miyamoto, K., and Ohta, H. (1990) Enzyme-mediated asymmetric decarboxylation of disubstituted malonic acids. *J. Am. Chem. Soc. 112*, 4077–4078.
12. Miyazaki, M., Kakidani, H., Hanzawa, S., and Ohta, H. (1997) Cysteine 188 revealed as being critical for the enzyme activity of arylmalonate decarboxylase by site-directed mutagenesis. *Bull. Chem. Soc. Jpn. 70*, 2765–2769.
13. Küttner, E. B., Keim, A., Kircher, M., Rosmus, S., and Sträter, N. (2008) Active-site mobility revealed by the crystal structure of arylmalonate decarboxylase from *Bordetella bronchiseptica*. *J. Mol. Biol. 377*, 386–394.
14. Okrasa, K., Levy, C., Hauser, B., Baudendistel, N., Leys, D., and Micklefield, J. (2008) Structure and mechanism of an unusual malonate decarboxylase and related racemases. *Chem.—Eur. J. 14*, 6609–6613.
15. Okrasa, K., Levy, C., Wilding, M., Goodall, M., Baudendistel, N., Hauer, B., Leys, D., and Micklefield, J. (2009) Structure-guided directed evolution of alkenyl and arylmalonate decarboxylases. *Angew. Chem., Int. Ed. 48*, 1–5.
16. Terao, Y., Miyamoto, K., and Ohta, H. (2006) Introduction of single mutation changes arylmalonate decarboxylase to racemases. *Chem. Commun. 34*, 3600–3602.
17. Miyamoto, K., and Ohta, H. (1992) Cloning and heterogeneous expression of a novel arylmalonate decarboxylase gene from *Alcaligenes bronchisepaticus* KU1201. *Appl. Microbiol. Biotechnol. 38*, 234–238.
18. Ueno, G., Kanda, H., Kumasaka, T., and Yamamoto, M. (2005) Beamline Scheduling Software: Administration software for automatic operation of the RIKEN structural genomics beamlines at SPring-8. *J. Synchrotron Radiat. 12*, 380–384.
19. Ueno, G., Hirose, R., Ida, K., Kumasaka, T., and Yamamoto, M. (2004) Sample management system for a vast amount of frozen crystals at SPring-8. *J. Appl. Crystallogr. 37*, 867–873.
20. Otwinowski, Z., and Minor, W. (1997) Processing of X-ray diffraction data collected in oscillation mode. *Methods Enzymol. 276*, 307–326.
21. Navaza, J. (1994) AMoRe: An automated package for molecular replacement. *Acta Crystallogr. A50*, 157–163.
22. Collaborative Computational Project, Number 4 (1994) The CCP4 suite: Programs for protein crystallography. *Acta Crystallogr. D50*, 760–763.
23. Murshudov, G. N., Vagin, A. A., and Dodson, E. J. (1997) Refinement of macromolecular structures by the maximum-likelihood method. *Acta Crystallogr. D53*, 240–255.
24. Alkema, W. B., Hensgens, C. M., Kroezinga, E. H., de Vries, E., Floris, R., van der Laan, J. M., Dijkstra, B. W., and Janssen, D. B. (2000) Characterization of the β-lactam binding site of penicillin acylase of *Escherichia coli* by structural and site-directed mutagenesis studies. *Protein Eng., Des. Sel. 13*, 857–863.
25. Alkema, W. B. L., Hensgens, C. M. H., Snijder, H. J., Keizer, E., Dijkstra, B. W., and Janssen, D. B. (2004) Structural and kinetic studies on ligand binding in wild-type and active-site mutants of penicillin acylase. *Protein Eng., Des. Sel. 17*, 473–480.
26. Duggleby, H. J., Tolley, S. P., Hill, C. P., Dodson, E. J., Dodson, G., and Moody, P. C. (1995) Penicillin acylase has a single-amino-acid catalytic centre. *Nature 373*, 264–268.
27. Brownlee, J. M., Carlson, E., Milne, A. C., Pape, E., and Harrison, D. H. (2006) Structural and thermodynamic studies of simple aldose reductase-inhibitor complexes. *Bioorg. Chem. 34*, 424–444.
28. Matsuoka, D., and Nakasako, M. (2009) Probability distributions of hydration water molecules around polar protein atoms obtained by a database analysis. *J. Phys. Chem. B 113*, 11274–11292.
29. Ruzheinikov, S. N., Taal, M. A., Sedelnikova, S. E., Baker, P. J., and Rice, D. W. (2005) Substrate-induced conformational changes in *Bacillus subtilis* glutamate racemase and their implications for drug discovery. *Structure 13*, 1707–1713.
30. Ohtaki, A., Nakano, Y., Iizuka, R., Arakawa, T., Yamada, K., Odaka, M., and Yohda, M. (2008) Structure of aspartate racemases complexed with a dual substrate analogue, citric acid, and implications for the reaction mechanism. *Proteins: Struct., Funct., Bioinf. 70*, 1167–1174.
31. Pillai, B., Cherney, M. M., Diaper, C. M., Sutherland, A., Blanchard, J. S., Vederas, J. C., and James, M. N. (2006) Structural insights into stereochemical inversion by diaminopimelate epimerase: An antibacterial drug target. *Proc. Natl. Acad. Sci. U.S.A. 103*, 8668–8673.
32. Dunathan, H. C. (1966) Conformation and reaction specificity in pyridoxal phosphate enzymes. *Proc. Natl. Acad. Sci. U.S.A. 55*, 712–716.
33. Wise, E. L., Yew, W. S., Gerlt, J. A., and Rayment, I. (2003) Structural evidence for a 1,2-enediolate intermediate in the reaction catalyzed by 3-keto-L-gulonate 6-phosphate decarboxylase, a member of the orotidine 5′-monophosphate decarboxylase suprafamily. *Biochemistry 42*, 12133–12142.
34. Dreyer, M. K., and Schulz, G. E. (1996) Catalytic Mechanism of the Metal-dependent Fuculose Aldolase from *Escherichia coli* as Derived from the Structure. *J. Mol. Biol. 259*, 458.
35. Brünger, A. T. (1993) Assessment of phase accuracy by cross validation: The free *R* value. Methods and applications. *Acta Crystallogr. D49*, 24–36.
36. Laskowski, R. A., MacArthur, M. W., Moss, D. S., and Thornton, J. M. (1993) PROCHECK: A program to check the stereochemical quality of protein structure. *J. Appl. Crystallogr. 26*, 283–291.
37. DeLano, W. L. (2002) The PyMOL Molecular Graphics System, DeLano Scientific, Palo Alto, CA.